Lasers in Surgery and Medicine 41:161–169 (2009)

Thermal Modeling and Experimental Validation of Human Hair and Skin Heated by Broadband Light

Feng Sun, PhD,[1] Alex Chaney,[1] Robert Anderson, PhD,[2] and Guillermo Aguilar, PhD[1]*
[1]*Department of Mechanical Engineering, University of California, Riverside, California 92521*
[2]*Aesthera Corp., Pleasanton, California 94588*

Background and Objective: In recent years, selective photothermolysis (PT) based on broadband light and assisted by skin vacuum (Photopneumatic Technology or PPx, by Aesthera) was introduced into the aesthetic market for epilation (hair removal) procedures. The present study aims to: (a) determine the overall effect of PPx on skin humidity and associated skin optical properties, and; (b) develop a PT numerical model to study the spatial and temporal hair and skin temperature variations during PPx epilation.
Methods: A customized cup was used to apply moderate vacuum for 10 seconds on the forearms and faces of five volunteers. Skin humidity was measured on test sites immediately after vacuum application. A selective PT model was developed and used to simulate transport of photons from a broadband light source into human skin. The PT model is experimentally validated using agar gel tissue phantoms. Systematic numerical simulations are carried out for fluences varying from 5.0 to 7.0 J/cm^2 and pulse durations varying from 2.5 to 25 milliseconds.
Results: Results of in vivo skin surface humidity measurements reveal that while absolute humidity varies between 30% and 75% between different volunteers and different locations, vacuum has a minimal effect on it. Experimental measurements of temperature variation during and after broadband light treatment agree well with model predictions. Numerical results indicate that average hair follicle temperature increases as a linear function of fluence. Longer pulse duration results in lower follicle temperature. However, immediately after each pulse, the temperature distribution within the hair follicle is highly non-uniform: the minimum temperature occurs at the follicle edge while the maximum is located between the center and edge of the follicle.
Conclusions: Vacuum appears to have minimal effect on skin humidity. The PT model developed and validated is expected to assist clinicians in the selection of broadband light treatment parameters to achieve optimal therapeutic outcomes during epilation procedures. Lasers Surg. Med. 41: 161–169, 2009. © 2009 Wiley-Liss, Inc.

Key words: hair removal; epilation; intense pulsed light; IPL; dermatology; selective photothermolysis; photopneumatic therapy; skin vacuum

INTRODUCTION

Flash lamps filled with either xenon or krypton xenon gas, emitting light with a broad wavelength spectrum ranging from 400 to 1,200 nm are widely applied in dermatologic practice, for example, epilation (removal of unwanted hair). Compared to conventional methods, for example, shaving, plucking, and waxing, epilation using broadband light is easy to perform with reduced pain, proven efficacy, and demonstrated satisfactory cosmetic outcome [1].

The mechanism of broadband light treatment is similar to the selective photothermolysis (PT) that Anderson and Parrish [2] proposed to describe the interactions between tissue and laser beams [1], although the selectivity extends to a wider spectrum of wavelengths and tissue depths [1,3]. Once delivered to skin, photons are selectively absorbed depending on their wavelengths by different pigmented tissue structures, for example, hair shaft and follicle, leading to rapid localized heating and various consequent biological events, for example, protein thermal denaturation. Epilation by broadband light is an alternative to laser technology with various advantages over many clinical lasers, such as the ability to deliver high fluences over larger areas compared to most clinical lasers, without the need of sophisticated laser generators, crystals and flash pumps. This makes the manufacturing of broadband light devices simpler and less expensive.

A successful broadband light epilation treatment requires careful management of treatment parameters. In recent years, some efforts have been devoted to reducing adverse effects, such as pain, transient erythema, purpura, crusting, and hyper- and hypopigmentation [1]. In particular, the use of moderate vacuum to stretch the skin during broadband light therapy has shown clinical success reducing pain due to the ensuing heat generation [4]. It has been hypothesized that the application of vacuum yields a cooling effect due to rapid evaporation of tissue water from the superficial skin layers [4]. If this hypothesis is true, the skin surface should show a significant increase in the heat transfer through it. Meanwhile, the tissue water concentration underneath should decrease, leading to a variation of the effective optical properties. The present paper studies the effect of vacuum on tissue water evaporation by in vivo

*Correspondence to: Guillermo Aguilar, PhD, Department of Mechanical Engineering, University of California, Riverside, CA 92521. E-mail: gaguilar@engr.ucr.edu
Accepted 28 December 2008
Published online in Wiley InterScience (www.interscience.wiley.com).
DOI 10.1002/lsm.20743

measurements of skin humidity on the forearms and faces of five volunteers.

Development of numerical PT models is another approach for better understanding and administration of light absorption therapy, while avoiding the adverse effects of broadband light treatment described above. Dermatologists would benefit from a model that requires patient-specific information (such as skin phototype and hair color) as inputs, to advise on the appropriate management of light treatment protocols, including the selection of pulse fluence and duration to achieve optimal therapeutic outcome.

Numerical modeling on the transport of high-intensity light in biological tissue has been the subject of extensive research since laser was widely applied in medical practice in the 1980s [5]. To date, Monte Carlo (MC) is the most widely and frequently used method regarded as the "gold standard" to describe the transport of photons in biological tissue [6]. MC is a flexible and descriptive, yet rigorous method to simulate photon transport. It addresses the "random walk" of photon propagation in a medium which involves scattering and absorption. Probability distributions are used to describe the step size of photon movement between photon-tissue interaction sites and the deflection angle for scattering. Using MC to simulate the propagation of monochromatic light in tissue, numerous works have been published in the past two decades [5,7–14].

Unlike single wavelength lasers, broadband light sources deliver polychromatic light with various intensities for different wavelengths. Since MC requires input of the optical properties of tissue, such as absorption and scattering coefficients and anisotropy factor (which are highly wavelength-dependent), implementation of MC code to study light-tissue interactions is challenging. Bäumler et al. [3] developed a diffusion approximation model to address the transport of light photons in human skin. In this work, the photon distribution was calculated for a series of discrete wavelengths within the spectrum and, thereafter, combined to calculate the temperature field of 2D skin tissue including epidermis, dermis and blood vessels.

The present study develops a numerical PT model using a MC code to compute the transport of photons, for example, propagation, scattering and absorption, within human skin. As a first order approximation, the optical properties of epidermis, dermis and hair are estimated by means of spectrum-intensity-weighted average. The output of the MC code provides the energy deposition, that is, heat source, for a subsequent heat diffusion (HD) computation via a finite difference code. This PT model (composed of MC and HD codes) is experimentally validated in vitro using agar gel as a tissue phantom, and then used to conduct a parametric study on pulse fluence and duration.

NUMERICAL MODEL

When light is aimed at skin, two primary physical processes occur: transport of photons in the tissue and subsequent heat diffusion. Therefore, the present PT model is composed of two interacting codes: MC and HD, which compute each of those physical events, respectively. Considering a cylindrical hair shaft vertical to the skin surface and rooted in the follicle, the calculation domain of the MC and HD codes is setup in a cylindrical coordinate system, which includes epidermis, dermis, hair shaft and follicle, as schematically shown in Figure 1. The thickness of epidermis and dermis is 70 μm and 3.43 mm, respectively. The radius of the modeled hair (r_h) is 0.1 mm and that of the follicle (r_{fo}) is 0.5 mm.

Monte Carlo (MC) Code

In this study, a MC code is implemented by revising the 3D modular adaptive grid numerical model developed by Pfefer et al. [11]. The effective optical absorption coefficient of epidermis, dermis and hair are estimated by means of spectrum-intensity-weighted average according to:

$$\mu_x = \mu_y \cdot vf_y \cdot sf_y + \mu_{water} \cdot vf_{water,x} \cdot sf_{water,x} \quad (1)$$

where μ is the estimated optical absorption coefficient; *vf* represents the volume fractions of water and chromophore, that is, blood and collagen for dermis and melanin for epidermis and hair, respectively; *sf* is the spectrum percentage absorbed by chromophore and water. Subscript x represents epidermis, dermis and hair, respectively; y represents the chromophore; and *water, x* represents the water in tissue x. Effective absorption coefficient of melanin, μ_{meln}, is computed (in cm^{-1}) by:

$$\mu_{meln} = \sum_{\lambda_0}^{1100} I_{meln}(\lambda)(1.7 \times 10^{12}\lambda^{-3.48}) \quad (2)$$

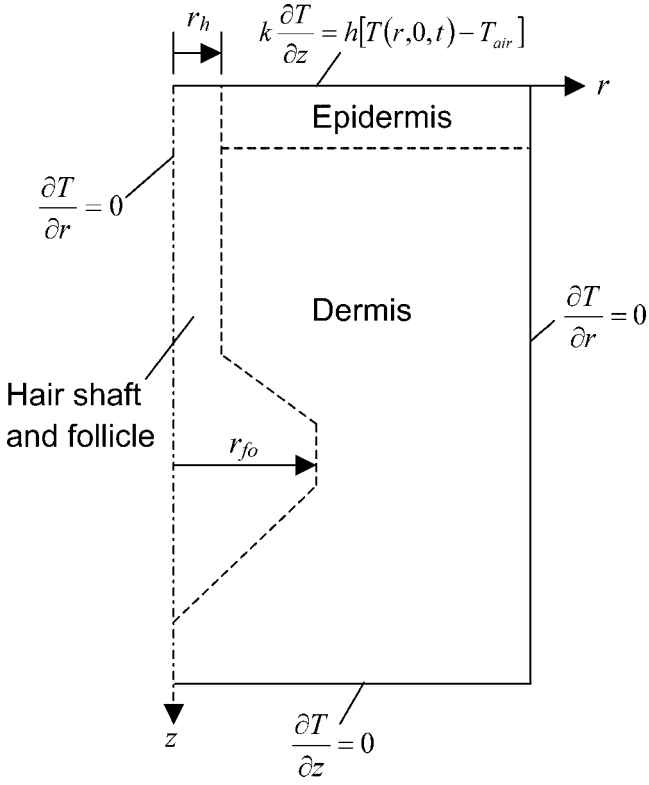

Fig. 1. Calculation domain of Monte Carlo and heat diffusion models.

where $I_{meln}(\lambda)$ is the normalized spectrum profile of the broadband light source that is absorbed by melanin, that is, the normalized intensities of each specific wavelength from λ_0, the cut-off filter wavelength to 1,100 nm, which satisfies:

$$\sum_{\lambda_0}^{1100} I_{meln}(\lambda) = 1 \quad (3)$$

In Equation (2), $(1.7 \times 10^{12}\lambda^{-3.48})$ is the spectrum-dependent absorption coefficient of melanin proposed by Jacques [15]. Similarly, the effective absorption coefficient of dermal blood and collagen, $\mu_{b,c}$ is computed (in cm^{-1}) by:

$$\mu_{b,c} = \sum_{\lambda_0}^{1000} I_{b,c}(\lambda)[\mu_{blood} \cdot vf_{blood} + \mu_{baseline}(1 - vf_{blood})] \quad (4)$$

where vf_{blood} is the volume fraction of blood and $I_{b,c}(\lambda)$ is the normalized spectrum profile of the broadband light source that is absorbed by dermal blood and collagen, which satisfies:

$$\sum_{\lambda_0}^{1000} I_{b,c}(\lambda) = 1 \quad (5)$$

Equation (4) uses $\mu_{baseline}$ to represent the absorption coefficient of bloodless dermis, which is primarily attributed to the light absorption by collagen and can be expressed as a function of wavelength [16]:

$$\mu_{baseline} = 7.84 \times 10^8 \lambda^{-3.255} \quad (6)$$

Meanwhile, the absorption coefficient of blood, μ_{blood}, is estimated according to:

$$\mu_{blood} = 0.5\mu_{Hb}(\lambda) + 0.5\mu_{HbO_2}(\lambda) \quad (7)$$

where $\mu_{Hb}(\lambda)$ is the absorption coefficient profile of deoxy-hemoglobin and $\lambda_{HbO_2}(\lambda)$ is that of oxy-hemoglobin [16]. In Equation (1), μ_{water} is calculated (in cm^{-1}) by:

$$\mu_{water} = \sum_{1000}^{3000} I_{water}(\lambda)\left[a \exp\left(-\frac{\lambda}{b}\right)\right] \quad (8)$$

where $I_{water}(\lambda)$ is the normalized spectrum profile of the broadband light source that is absorbed by water, which satisfies:

$$\sum_{1000}^{3000} I_{water}(\lambda) = 1 \quad (9)$$

In Equation (8), $[a \exp(-\lambda/b)]$ is the exponential regression of the absorption coefficient profile in the range of 1,000–3,000 nm, which is believed to be absorbed primarily by water. This spectrum-intensity-weighted average approach is applied to estimate the effective absorption coefficient for epidermis, dermis, and hair.

Finally, the effective scattering coefficient is calculated (in cm^{-1}) by:

$$\mu_s = \sum_{\lambda_0}^{1000} I(\lambda)(2 \times 10^5 \lambda^{-1.5} + 2 \times 10^{12}\lambda^{-4}) \quad (10)$$

TABLE 1. Baseline Parameters Used in Monte Carlo Code: Effective Optical Properties Estimated by Spectrum-Intensity-Weighted Average

	Epidermis	Dermis	Hair
Melanin volume concentration	0.10	n/a	0.30
Water volume concentration	0.05	0.05	0.25
Absorption coefficient (cm^{-1})	12.15	1.00	36.61
Scattering coefficient (cm^{-1})	13.45	13.45	13.45
Refractive index	1.37	1.37	1.37
Anisotropy	0.79	0.79	0.79

where $I(\lambda)$ is the normalized intensity of the broadband light source for specific wavelength, which satisfies:

$$\sum_{\lambda_0}^{1000} I(\lambda) = 1 \quad (11)$$

In Equation (10), $2 \times 10^5 \lambda^{-1.5}$ and $2 \times 10^{12}\lambda^{-4}$ represent the contributions from Mie scattering due to collagen fibers and from Rayleigh scattering due to small tissue structures, respectively [17]. It should be noted that in Equations (1–11), the unit for wavelength (λ) is nm.

Applying this spectrum-intensity-weighted average method and considering the cut-off wavelength, λ_0, to be 500 nm, the effective optical properties of epidermis, dermis and hair are shown in Table 1.

Finite Difference Heat Diffusion (HD) Code

During broadband light exposure, absorption of photons by skin converts the energy deposition into heat, resulting in a heat diffusion process which can be described as follows.

$$\frac{\partial T_x(r,z,t)}{\partial t} = \alpha_x \nabla^2[T_x(r,z,t)] + [Q_x(r,z,t)] \quad (12)$$

where T is temperature (°C), t is time (seconds), α is the thermal diffusivity of tissue (1.042×10^{-7} m^2/second for epidermis, 1.27×10^{-7} m^2/second for dermis and 1.13×10^{-7} m^2/second for hair shaft and follicle [18]) and Q is the heat generation due to absorption of photons (W/m^3), which is provided by the MC code. In Equation (12), , the subscript, x, is used to represent various tissue components considered herein: epidermis, dermis and hair, respectively. Considering that skin surface temperature is usually lower than normal body temperature (37°C), the initial temperature of the HD code is defined as follows.

$$T(r,z,0) = \begin{cases} 32 & z = 0 \\ 32 + \frac{z}{2}(37 - 32) & 0 < z \le 2 \text{ mm} \\ 37 & z > 2 \text{ mm} \end{cases} \quad (13)$$

Equation (13) assumes an initial temperature of 32°C at the skin surface ($z = 0$) which increases linearly to 37°C at z = 2 mm, after which it remains constant.

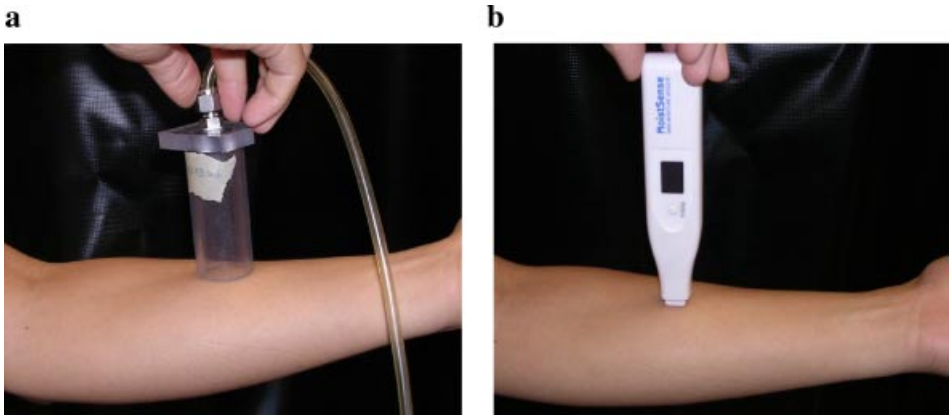

Fig. 2. In vivo experiments to determine the effects of vacuum on skin humidity: (**a**) application of vacuum; (**b**) measurement of skin humidity.

In the HD code, the skin surface is subject to a convective thermal boundary condition with a constant heat transfer coefficient, h:

$$k\frac{\partial T}{\partial z} = h[T(r,0,t) - T_{\text{air}}] \tag{14}$$

where k is the conductivity of hair or epidermis, h is the heat transfer coefficient, and T_{air} is the ambient temperature (20°C). Central axis, z, is subject to an axisymmetric boundary condition, while the lower and right boundaries are assumed adiabatic (i.e., modeled unit is assumed to be repetitive). The above mathematic model was discretized and solved by an explicit finite difference code, in which the stability conditions for the skin surface nodes are defined as follows:

$$\text{Fo}(1 + \text{Bi}) < \frac{1}{4} \tag{15}$$

where Fo and Bi are the finite-difference forms of the Fourier and Biot numbers, which are calculated according to:

$$\text{Fo} = \frac{\alpha \cdot \Delta t}{(\Delta r)^2} \tag{16}$$

$$Bi = \frac{h \cdot \Delta r}{k} \tag{17}$$

In Equations (16) and (17), Δt is time step, k is thermal conductivity of tissue (W/m-K) and Δr is the mesh size. This stability condition is also met for interior nodes to avoid instabilities and ensure convergence.

EXPERIMENTAL MATERIALS AND METHODS

Exploring Effect of Vacuum on Skin Humidity by In Vivo Tests

To study the effect of vacuum on tissue water evaporation, in vivo experimental tests were performed on five volunteers' forearms and faces. As shown in Figure 2a, a vacuum cup was used to apply moderate vacuum of −16.93 kPa (−5″ Hg) for 10 seconds. The skin humidity was then measured immediately after the vacuum application using MoistSense (Moritex U.S.A., Inc., San Jose, CA), a skin humidity sensor with full scale of 100, as shown in Figure 2b. The tests were repeated 10 times for each volunteer. It should be noted that volunteer 3 could not participate in the face humidity measurements, and thus was replaced by volunteer 6.

Experimental Setup for PT Model Validation

To validate the aforementioned numerical PT model, an experiment was performed to measure temperature variation in a two-layer, agar gel skin phantom, subject to light exposure. Difco™ granulated agar, purchased from Voigt Global Distribution LLC (Lawrence, KS) was used for tissue phantom preparation. Two dyes: Direct Red 81, obtained from Aldrich Chemical Co. (Milwaukee, WI) and Chinese ink were used to vary the effective absorption coefficient of the different tissue structures. According to Table 2, agar gel suspensions were prepared by dissolving the granulated agar, dyes, and full milk into boiling distilled water. The concentrations of the dyes were determined experimentally so that the measured effective absorption coefficients of 1-mm-thick agar gel slides irradiated with light were the same as those estimated for epidermis and dermis by Equation (1).

The dyed agar gel suspensions were filled into an acrylic cylindrical mold, in which a thermocouple (CO2-K type, Omega, Stamford, CT) was fixed at a predetermined position. With a 0.05 mm (0.002″) thick foil junction, this thermocouple is recommended for extremely fast temperature measurements. The thermocouple signal was acquired

TABLE 2. Components of Epidermal and Dermal Phantoms (Rest Is Water)

	Granulated agar (%)	Dye	Milk (%)
Epidermis phantom	2	0.5% Chinese Ink	1
Dermis phantom	2	2.467×10^{-5} M Direct Red 81	1

by a LABVIEW system (National Instrument, Austin, TX), triggered by the signal from a photodiode, via a DAQ board. During the experiment, 1-pulse, 2-pulse, and 3-pulse broadband light pulse sequences were launched by a Photopneumatic™ (PPx) system (Aesthera Corp., Pleasanton, CA), with 2.5 milliseconds duration for each pulse and 200-millisecond intervals between consecutive pulses. Cumulative light fluence was measured by a customized broadband light energy meter, Comet IPL-30 × 15 (Ophir, Jerusalem, Israel). The experimental system is schematically shown in Figure 3.

Concurrently, the PT model was used to simulate the same experimental scenario, where the thermal diffusivity of tissue phantoms (dyed agar gel) was assumed to be that of water. Comparisons were then made between the experimentally measured temperature variations of the tissue phantom and those predicted by the numerical model.

Experimental Data Processing

During the experiments, tissue phantoms and the thermocouple are exposed to light irradiation, which will induce an artifact in the thermocouple signal due to the direct absorption of light by the thermocouple bead. To reduce the exposure area and minimize this artifact, the thermocouple was fixed perpendicular to the irradiated surface. In addition, we applied an algorithm proposed by Manns et al. [19] to quantify this artifact. The algorithm assumes that the recorded temperature increase can be expressed as follows:

$$\Delta T(t) = A\left[1 - \exp\left(-\frac{t}{\tau}\right)\right] + Bt \qquad (18)$$

where $\Delta T(t)$ is the temperature increase recorded by the thermocouple, the exponential term on the right hand side of the equation represents the temperature increase due to direct absorption of light by the thermocouple, and B (°C/second) is the slope of the linear temperature increase due to the absorption of light by the medium, that is, tissue phantoms. Applying Equation (18), one can quantify and remove the artifact via a regression through experimental data.

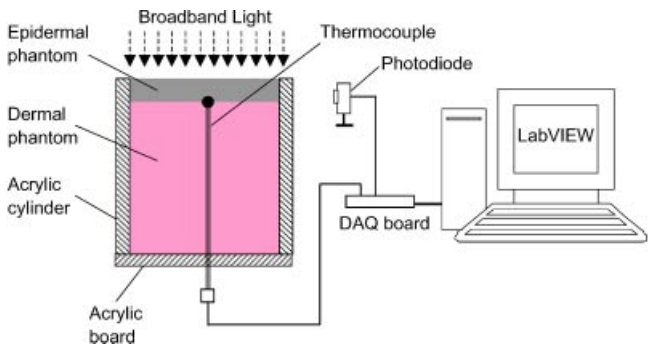

Fig. 3. Schematic of experimental setup to validate numerical model.

RESULTS AND DISCUSSION

Effect of Vacuum on Skin Humidity

Figure 4 shows the results of skin humidity before and after (shaded columns) the application of vacuum, where Figure 4a shows the results measured from volunteers' forearms while Figure 4b shows the results from faces. Paired and two-tailed Student's t-tests were performed to analyze the forearm and face data, respectively. The statistic analyses indicate that the application of vacuum does not show a consistent and significant effect on skin humidity (P-value is 0.1432 for forearm and 0.4028 for face). As a result, the application of vacuum is believed to have minimal effect on tissue water concentration, which may therefore be treated as a constant during the estimation of optical properties. Also, because of this fact, it is reasonable to assume a constant and relatively low convective heat transfer coefficient, h (10 W/m^2-K) [20], as the boundary condition in Equation (14).

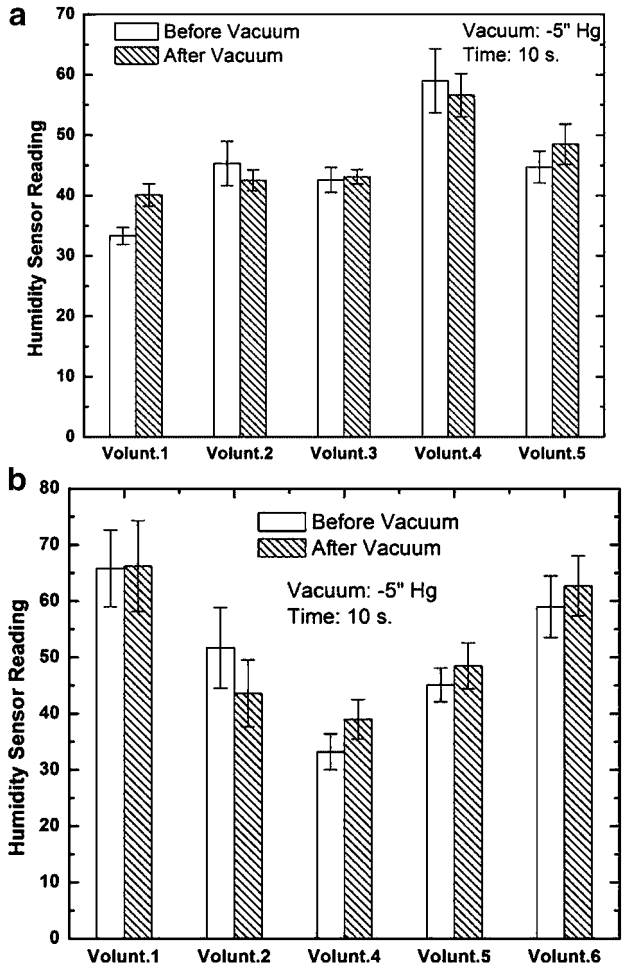

Fig. 4. Results of in vivo experiments exploring the effects of vacuum on skin surface humidity: (**a**) results from forearm; (**b**) results from face.

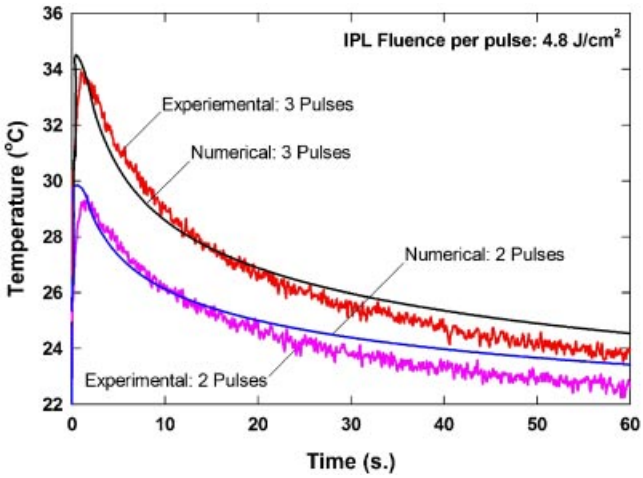

Fig. 5. Comparison of experimental and numerical results: temperature variation at predetermined position in two-layer tissue phantom during and after IPL pulses.

Validation of PT Model

In order to validate the numerical PT model, experimental measurements were carried out. The purpose was to study the temperature variation at a predetermined position in a two-layer agar gel. The comparison between the experimental results and the numerical model predictions is shown in Figure 5. As seen, experimental and numerical results agree well for both 2-pulse and 3-pulse light sequences. The agreement indicates that the MC code provides accurate heat source information to the HD code. One can also see that as the tissue phantom is cooling, for example, $t > 30$ seconds, the experimental results become slightly lower than the numerical results. The reason for this difference may be that the heat lost from the tissue phantom through the acrylic walls is neglected in the numerical simulation, because it assumes adiabatic thermal boundaries for the bottom and side walls (see Figs. 1 and 3).

Temperature Map During Broadband Light Therapy

Figure 6 shows the calculated temperature map of tissue when subjected to a three-pulse light sequence, where the three maps (a, b, and c) represent the time immediately after the 1st, 2nd, and 3rd pulses, respectively. In the calculation, the fluence per pulse is 4.8 J/cm^2, which is the lowest energy density delivered by the PPx system. It can be seen that temperature distribution in the calculation domain is highly non-uniform: hair follicle and epidermis show higher temperature than dermis. This result can be understood by considering three factors: (1) effective absorption coefficient, (2) tissue spatial orientation with respect to light incidence direction, and (3) distance to the light source. For example, the maximum temperature always occurs at the upper-left corner of the domain, that is, the tip of the hair shaft, since it has a high absorption coefficient (36.61 cm^{-1}), is directly irradiated by the photons, and the closest to the light source. In contrast, the follicle at the bottom of the hair shaft is the farthest away from the light source, so it always shows a lower temperature. Interestingly, the overall temperature in the follicle is higher than that in the hair shaft between 0.5 and 2 mm below the surface. The reason is that the hair shaft is parallel to the light incidence direction. As a result, photons passing through the epidermis ($0.1 \text{ mm} < r < 0.5 \text{ mm}$) have minimal opportunity to propagate into the hair shaft unless they are highly scattered, but they can readily be absorbed by the protruding follicle.

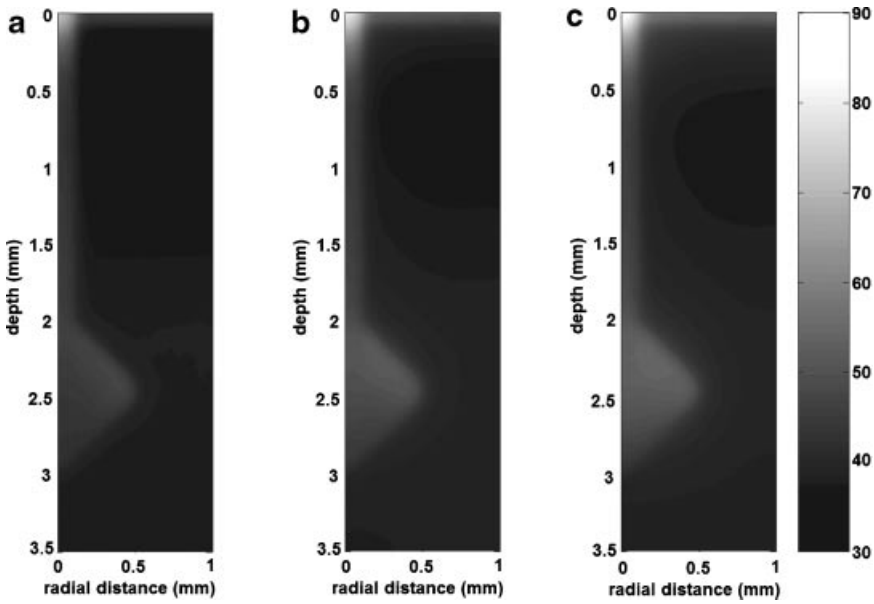

Fig. 6. Calculated temperature map: (**a**) after 1st pulse; (**b**) after 2nd pulse; (**c**) after 3rd pulse (IPL fluence per pulse is 4.8 J/cm^2).

Temperature Distribution Along the Central Axis

Temperature distribution in the modeled hair and follicle is one of our primary study interests. Figure 7 shows the temperature distribution along the central axis of the domainafter the 3rd pulse ($t = 407.5$ milliseconds), where light fluences are 5.0, 6.0, and 7.0 J/cm^2, respectively. The gray insert outlines the geometry and position of the modeled hair and follicle, which helps to locate the temperature profile along the central axis. As seen, the calculated temperature distribution is not as smooth as a deterministic model would predict, since the MC code is a stochastic and descriptive method and thus its outcome includes slight randomness. It is not surprising that the temperature of the modeled hair and follicle increases as light fluence increases from 5.0 to 7.0 J/cm^2. It can also be seen that along the central axis, the maximum temperature occurs at $z = 0$, and a large temperature gradient exists between $0 \le z \le 0.5$ mm, which is consistent with the temperature map of Figure 6c. Within the follicle (2.0 mm $\le z \le$ 2.5 mm), the temperature profile shows a local temperature maximum. In order to study the effect of fluence on the follicle, we define an average follicle temperature, $\bar{T}_{\text{fol}}$, as follows:

$$\bar{T}_{\text{fol}} = \frac{1}{n}\sum_{i=1}^{n} T_i \tag{19}$$

where n is the total number of temperature data points at 2.0 mm $\le z \le$ 2.5 mm, that is, z_{avg}, as indicated in the figure.

Parametric Study

A successful light based treatment requires a careful management of parameters to avoid potential adverse effects and concomitant reactions, for example, erythema which is always accompanied by edema, purpura, crusting, hyper-, and hypopigmentation [1]. The primary parameters include *fluence* and *pulse duration*. Figure 8 shows the

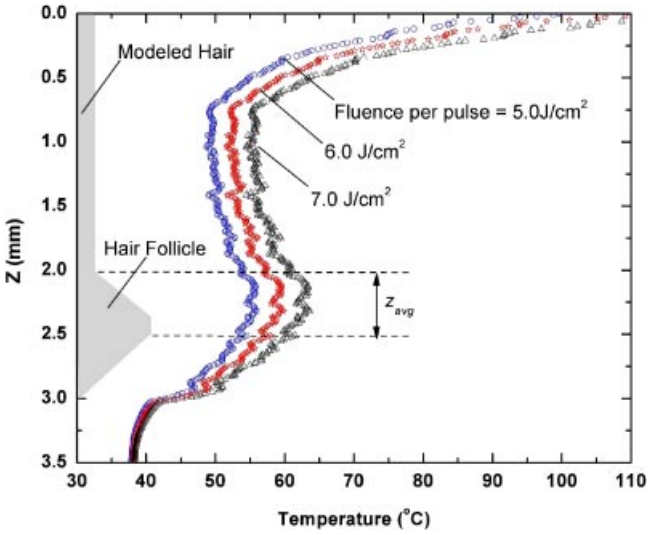

Fig. 7. Temperature distribution along central axis after 3rd pulse.

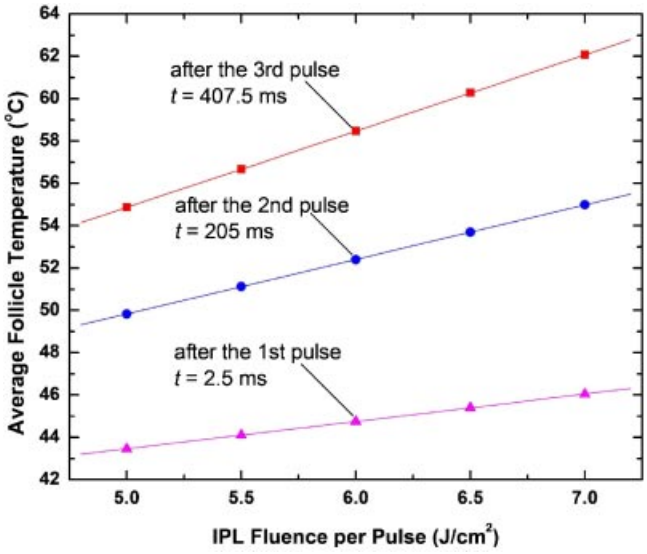

Fig. 8. Effect of IPL fluence on average follicle temperature.

effect of fluence on $\bar{T}_{\text{fol}}$ after the 1st, 2nd, and 3rd pulse, respectively. It can be seen that $\bar{T}_{\text{fol}}$ increases with fluence according to a linear function:

$$\bar{T}_{\text{fol}} = a + b \cdot E_{\text{f}} \tag{20}$$

where E_{f} is the fluence per pulse in J/cm^2. Values of a and b can be obtained from data regression as shown in Table 3. One can see that when E_{f} is zero, $\bar{T}_{\text{fol}}$ is approximately 37°C, the initial temperature for the tissue more than 2 mm deep, which is reasonable.

Besides fluence, another critical parameter is the *pulse duration*. A series of calculations have been conducted considering different pulse durations. Figure 9 shows the follicle temperature distribution along a horizontal line (see insert in figure) in the follicle after the 3rd light pulse, when the fluence per pulse is 7.0 J/cm^2 and pulse duration, t_{p}, is 10, 15, 20, and 25 milliseconds, respectively.

From Figure 9 one can see that the follicle temperature decreases as pulse duration increases, since the longer pulse duration results in reduced pulse power, that is, pulse energy per unit time, and allows longer time for heat diffusion between the heated follicle and the surrounding dermal tissue. On the other hand, it can be seen that for each temperature profile, the temperature increases gradually

TABLE 3. Linear Regression Results for Coefficients a and b in Equation (20)

	a (°C)	b (°C-cm^2/J)	SD (°C)
1st pulse ($t = 2.5$ milliseconds)	36.998	1.292	5.453×10^{-5}
2nd pulse ($t = 205$ milliseconds)	36.930	2.579	1.432×10^{-5}
3rd pulse ($t = 407.5$ milliseconds)	36.869	3.599	3.856×10^{-5}

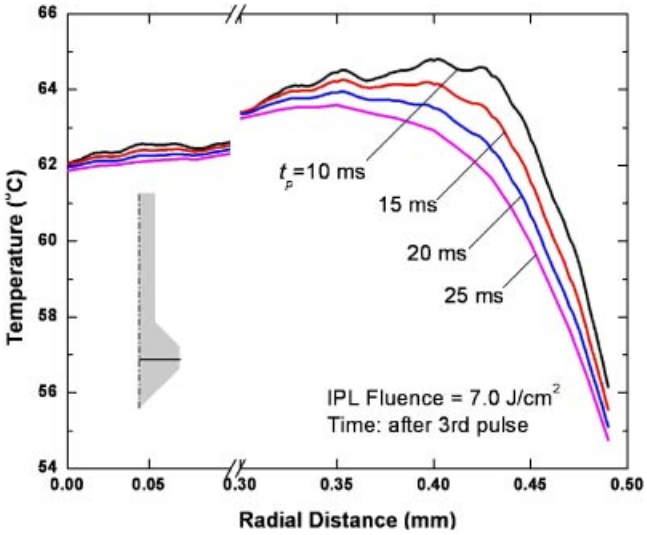

Fig. 9. Temperature distribution along a horizontal line after 3rd pulse when the pulse duration, t_p, is 10, 15, 20, and 25 milliseconds, respectively.

with r, reaches a maximum for r in the range of 0.35–0.40 mm, and then quickly drops down as r keeps increasing to 0.5 mm, that is, toward the edge of the follicle.

In addition to pulse fluence and duration, extensive studies will be conducted on patient-dependent parameters, including the concentrations of melanin and water in epidermis and hair, which are used to quantify and estimate the optical properties of target tissue. These results will be reported shortly in a follow-up paper.

CONCLUSIONS

A photothermolysis (PT) model was developed to study broadband light treatment for epilation (hair removal). Photon propagation and energy deposition are described by a MC code, which provides the heat source for a HD code, solved by finite difference method. Together, the MC and HD codes conform the PT model. For a first order approximation, optical parameters of target tissue, for example, effective absorption coefficients and scattering coefficients of epidermis, dermis and hair, are estimated by means of spectrum-intensity-weighted average. Experiments were conducted to explore the effect of vacuum on tissue water concentration and validate the PT model. Applying the PT model, parametric studies were subsequently carried out to determine the effects of light pulse fluence and duration.

In vivo experimental results of skin surface humidity reveal that the vacuum has minimal effect on tissue water concentration. Using agar gel as a tissue phantom, experimental measurements of temperature variation during and after broadband light treatment agree well with model predictions. Results of parametric studies indicate that the average temperature of the hair follicle increases as a linear function of light pulse fluence. Longer pulse duration results in decreased follicle temperature. Immediately after each light pulse, the temperature distribution within the hair follicle is highly non-uniform: the minimum temperature occurs at the follicle edge while the maximum is located between the center and edge of the follicle. The PT model developed and validated is expected to assist clinicians in the selection of broadband light treatment parameters to achieve optimal therapeutic outcomes during epilation procedures.

ACKNOWLEDGMENTS

The authors appreciate the financial and technical support provided by Aesthera Co. (Pleasanton, CA).

REFERENCES

1. Raulin C, Greve B, Grema H. IPL technology: A review. Laser Surg Med 2003;32:78–87.
2. Anderson RR, Parrish JA. Selective photothermolysis: Precise microsurgery by selective absorption of pulsed radiation. Science 1983;220:524–527.
3. Bäumler W, Vural E, Landthaler M, Muzzi F, Shafirstein G. The effects of intense pulsed light (IPL) on blood vessels investigated by mathematical modeling. Laser Surg Med 2007;39:132–139.
4. Jacques SL, Naruikar VA, Anderson R. The optics of stretching skin and use during clinical laser treatments. Progress report, prepared for distribution at American Academy of Dermatology, 2005 Feb. 18–22; New Orleans, LA.
5. Wilson BC, Adam G. A Monte Carlo Model for the absorption and flux distributions of light in tissue. Med Phys 1983;10: 824–830.
6. Binzoni T, Leung TS, Giust R, Rufenacht D, Gandjbakhche AH. Light transport in tissue by 3D Monte Carlo: Influence of boundary voxelization. Comput Meth Prog Bio 2008;89:14–23.
7. Keijzer M, Jacques SL, Prahl SA, Welch AJ. Light distributions in artery tissue—Monte-Carlo simulations for finite-diameter laser-beams. Laser Surg Med 1989;9:148–154.
8. Wang LH, Jacques SL. Hybrid model of Monte-Carlo simulation and diffusion-theory for light reflectance by turbid media. J Opt Soc Am A 1993;10:1746–1752.
9. Wang LH, Jacques SL, Zheng LQ. MCML—Monte Carlo modeling of light transport in multilayered tissues. Comput Meth Prog Bio 1995;47:131–146.
10. Jacques SL, Wang LH. Monte Carlo modeling of light transport in tissues. In: Welch AJ, Van Gemert MJC, editors. Optical-thermal response of laser-irradiated tissue. New York and London:Plenum Press; 1995:73–100.
11. Pfefer TJ, Barton JK, Chan EK, Ducros MG, Sorg BS, Milner TE, Nelson JS, Welch AJ. A three-dimensional modular adaptable grid numerical model for light propagation during laser irradiation of skin tissue. IEEE J Sel Top Quant 1996;2: 934–942.
12. Barton JK, Pfefer TJ, Welch AJ, Smithies DJ, Nelson JS, van Gemert MJC. Optical Monte Carlo modeling of a true port wine stain anatomy. Opt Express 1998;2:391–396.
13. Boas DA, Culver JP, Stott JJ, Dunn AK. Three dimensional Monte Carlo code for photon migration through complex heterogeneous media including the adult human head. Opt Express 2002;10:159–170.
14. Zhang R, Verkruysse W, Aguilar G, Nelson JS. Comparison of diffusion approximation and Monte Carlo based finite element models for simulating thermal responses to laser irradiation in discrete vessels. Phys Med Biol 2005;50: 4075–4086.
15. Jacques SL. Origins of tissue optical properties in the UVA, visible and NR regions. In: Alfano RR, Fujimoto JG, editors. Advances in optical imaging and photon migration, Vol. 2.Washington, DC:OSA; 1996:364–370.

16. Oregon Medical Laser Center. Webpage: http://omlc.ogi.edu/index.html.
17. Saidi IS, Jacques SL, Tittel FK. Mie and Rayleigh modeling of visible-light scattering in neonatal skin. Appl Optics 1995;34:7410–7418.
18. Duck FA, editor. Physical properties of tissue: A comprehensive reference book. London, San Diego: Academic Press; 1990.
19. Manns F, Milne PJ, Gonzalez-Cirre X, Denham DB, Parel JM, Robinson DS. In situ temperature measurements with thermocouple probes during laser interstitial thermotherapy (LITT): Quantification and correction of a measurement artifact. Laser Surg Med 1998;23:94–103.
20. Incropera FP, Dewitt DP, Bergman TL, Lavine AS. Introduction to heat transfer.John Whiley & Sons; 2007.